ORIGINAL ARTICLE

Meridionally Extending Anomalous Wave Train over Asia During Breaks in the Indian Summer Monsoon

Uppara Umakanth[1] · Ramesh K. Vellore[1] · R. Krishnan[1] · Ayantika Dey Choudhury[1] · Jagat S. H. Bisht[1,2] · Giorgia Di Capua[3,4] · Dim Coumou[3,4] · Reik V. Donner[3,5]

Abstract

Anomalous interactions between the Indian summer monsoon (ISM) circulation and subtropical westerlies are known to trigger breaks in the ISM on subseasonal time-scales, characterised by a pattern of suppressed rainfall over central-north India, and enhanced rainfall over the foothills of the central–eastern Himalayas (CEH). An intriguing feature during ISM breaks is the formation of a mid-tropospheric cyclonic circulation anomaly extending over the subtropical and mid-latitude areas of the Asian continent. This study investigates the mechanism of the aforesaid Asian continental mid-tropospheric cyclonic circulation (ACMCC) anomaly using observations and simplified model experiments. The results of our study indicate that the ACMCC during ISM breaks is part of a larger meridional wave train comprising of alternating anticyclonic and cyclonic anomalies that extend poleward from the monsoon region to the Arctic. A lead–lag analysis of mid-tropospheric circulation anomalies suggests that the meridional wave-train generation is linked to latent heating (LH) anomalies over the CEH foothills, Indo-China, and the Indian landmass during ISM breaks. By conducting sensitivity experiments using a simplified global atmospheric general circulation model forced with satellite-derived three-dimensional LH, it is demonstrated that the combined effects of the enhanced LH over the CEH foothills and Indo-China and decreased LH over the Indian landmass during ISM breaks are pivotal for generating the poleward extending meridional wave train and the ACMCC anomaly. At the same time, the spatial extent of the mid-latitude cyclonic anomaly over Far-East Asia is also influenced by the anomalous LH over central–eastern China. While the present findings provide interesting insights into the role of LH anomalies during ISM breaks on the poleward extending meridional wave train, the ACMCC anomaly is found to have important ramifications on the daily rainfall extremes over the Indo-China region. It is revealed from the present analysis that the frequency of extreme rainfall occurrences over Indo-China shows a twofold increase during ISM break periods as compared to active ISM conditions.

Keywords Indian summer monsoon · Active and break periods · Meridional Rossby wave · Monsoon and mid-latitude flows · Extreme precipitation

1 Introduction

The active and break monsoon cycles of the Indian summer monsoon (ISM) rainfall variability are a well-known aspect of the monsoon subseasonal variability and have

✉ R. Krishnan
krish@tropmet.res.in

[1] Centre for Climate Change Research, Indian Institute of Tropical Meteorology, Pune 411 008, India

[2] Research and Development Centre for Global Change, Japan Agency for Marine Earth Science Technology, Yokohama, Japan

[3] Potsdam Institute for Climate Impact Research, Potsdam, Germany

[4] Institute for Environmental Studies, Vrije Universiteit, Amsterdam, The Netherlands

[5] Department of Water, Environment, Construction and Safety, Magdeburg-Stendal University of Applied Sciences, Magdeburg, Germany

been extensively studied by various researchers (e.g., Ramamurthy 1969; Raghavan 1973; Krishnamurti et al. 1989; Krishnan et al. 2000, 2009; Annamalai and Slingo 2001; Gadgil and Joseph 2003; Krishnamurthy and Kinter 2003; Rajeevan et al. 2010; Umakanth et al. 2014). One of the salient features of break periods in the ISM is the anomalous enhancement of rainfall activity along the southern slopes of central and eastern parts of the Himalayas (CEH), and also notably over the Indo-Chinese peninsular countries (e.g., Dhar et al. 1984; Dhar and Nandargi 2000; Krishnan et al. 2009; Ramesh Kumar et al. 2009; Vellore et al. 2014). Furthermore, precipitation enhancements over the CEH foothills during the ISM break periods are well recognised to have associations with the northward migration of the monsoon trough (Ramamurthy 1969), enhanced moisture convergence by the southerly flow from the Bay of Bengal (BoB, Vellore et al. 2014), and equatorward advancing large-amplitude troughs in the upper level westerlies (e.g., Ramaswamy 1962; Krishnan et al. 2000). Earlier studies have reported the presence of anomalous cyclonic circulation at upper levels on a planetary scale spanning the Asian mid-latitudes during weak phases of the ISM (e.g., Keshavamurthi and Awade 1974; Raman and Rao 1981; Krishnan and Sugi 2001; Krishnan et al. 2009). Vellore et al. (2014) further noted that the vorticity enhancement over the CEH foothill region during ISM breaks was associated with an eastward progression of 500 hPa height perturbations towards the southern part of the Tibetan Plateau.

Subseasonal fluctuations of ISM precipitation and associated diabatic heating are known to modulate the zonal and meridional propagation characteristics of monsoon intra-seasonal oscillations (ISOs, Hazra and Krishnamurthy 2015). Yasunari (1986) suggested that diabatic heating fluctuations over the ISM environment can induce low-frequency oscillatory behaviour of the extra-tropical upper level westerlies on intra-seasonal time-scales. A major component of diabatic heating over the tropics and monsoon dominated areas involves LH release from organised convection (e.g., Houze 1997; Yanai and Tomita 1998; Schumacher et al. 2004; Houze et al. 2007; Krishnamurti et al. 2010; Choudhury et al. 2018). Studies have noted that interactions between the LH from the Asian monsoon precipitation and the mean subtropical westerly flow environment can generate a westward extending stationary Rossby waves, leading to pronounced summer-time descent over the Mediterranean and Sahara regions (Rodwell and Hoskins 1996; Liu et al. 2001). Conversely, eastward propagation of mid-latitude Rossby wave trains originating from the Atlantic can also modulate the rainfall fluctuations over the northwestern part of the Indian subcontinent on intra-seasonal time-scales (Ding and Wang, 2007, 2009; Saeed et al. 2011a).

Furthermore, teleconnections between the ISM and circulation over East Asia have also been noted in connection with setting up of a quasi-stationary Rossby wave pattern along the upper level Asian jet in response to ISM heating (e.g., Kripalani et al. 1997; Krishnan and Sugi 2001; Enomoto et al. 2003). Stan et al. (2017) have recently provided a comprehensive review of the current scientific understanding, as well as the gap areas, related to various aspects of tropical and extra-tropical interactions on intra-seasonal time-scales.

An important aspect of Rossby wave-train excitation in response to diabatic heating over the tropics and monsoon areas is the formation of meridionally extending patterns of large-scale circulation anomalies towards the extra-tropics and polar latitudes (e.g., Sardeshmukh and Hoskins 1988; Liu et al. 2001; Enomoto et al. 2003; Krishnan et al. 2009, Krishnamurti et al. 2015). While a decrease in upper tropospheric divergence during ISM breaks due to suppressed monsoon convection over the Indian subcontinent can induce a downstream Rossby wave response towards East Asia (Krishnan et al. 2009), it is not yet clear if the monsoonal heating anomalies can have any further consequences on large-scale circulation patterns. Murata et al. (2017) noted that extreme rain periods over Cherrapunji, the wettest place on Earth located over the CEH, had associations with westward propagating low-level circulation anomalies from the western North Pacific. Their results further indicated that a large number of extreme rain periods over Cherrapunji were coincident with ISM breaks. While taking note of the aforesaid studies, it must be mentioned that several aspects of the coupled interplay between the ISM heating and large-scale circulation variations on intra-seasonal time-scales over the broader Asian monsoon region and extra-tropics are not fully understood. This study intends to focus on the large-scale circulation response to LH variations during ISM breaks through the use of observations and model simulations. Details about the data sets and numerical experiments are described in the following section.

2 Data Sets and Model Details

The study utilises the observed and reanalyzed data products of precipitation and the circulation for the months of June–July–August–September during ISM season. The precipitation data sets include the APHRODITE (Yatagai et al. 2009, 2012) daily rainfall gridded data (0.25°×0.25° horizontal grid resolution) for the period 1979–2007, and Tropical Rainfall Measuring Mission (TRMM) 3B42 daily rainfall estimates over the global tropics (50°S–50°N; archived at 0.25°×0.25°) for the period 1998–2014. The algorithm 3B42 combines TRMM and the ground-truth rain gauge data sets (Huffman et al. 1995, 1997). The IMD gridded rainfall data (0.25°×0.25° horizontal grid resolution) by Pai et al. (2014) are used for the period 1979–2014 to infer

the active and break ISM cases. The criterion for active and break ISMs is based on the method by Rajeevan et al. (2010) using the standardised rainfall anomalies over central India (68°E–88°E and 18°N–28°N) (see Table 1). ERA-Interim reanalysed daily precipitation and three-dimensional gridded circulation products (archived at 0.75° × 0.75° resolution) for the period 1979–2014 used in this study are obtained from the European Centre for Medium Range Weather Forecasts (ECMWF) (Simmons et al. 2007; Dee et al. 2011).

Table 1 List of break spells for the period 1979–2014. Only the spells which last for at least 5 consecutive days are considered for the analysis. Here, the symbol J represents July and A represents August

	Spells with period ≥ 5 days
Year	Break
1979	2–7J, 14–29A
1980	–
1981	–
1982	1–8J
1983	–
1984	–
1985	–
1986	23–31A
1987	30J–4A, 9–13A
1988	–
1989	30J–3A
1990	–
1991	–
1992	4–10J
1993	8–13A, 22–28A
1994	–
1995	3–7J, 11–17A
1996	–
1997	11–15J, 9–17A
1998	20–26J, 16–21A
1999	1–5J, 12–18A
2000	29J–8A
2001	–
2002	4–16J, 22–31J
2003	
2004	26–31A
2005	8–14A, 24–31A
2006	
2007	18–23J
2008	16–21J
2009	29J–10A
2010	–
2011	–
2012	–
2013	–
2014	15–21A

The atmospheric general circulation model (GCM) used in this study is only for the purpose of understanding the thermally driven large-scale circulation response to imposed heating in a forced-damped setup. Therefore, the complex representations of physical processes and boundary forcing are excluded for simplicity. The model is forced with observed three-dimensional heating and steady-state solutions are constructed by integrating the model. The model starts from rest state and the initial three-dimensional thermal state of the atmosphere is set to the global mean values of temperature. The dynamical core of this model is based on a spectral formulation (Bourke 1974) having a rhomboidal truncation at zonal wavenumber 40 (R40), which corresponds to a Gaussian grid with an approximately horizontal resolution of 2.835° (longitude) and 1.76° (latitude) and employs sigma coordinates in the vertical direction with 25 vertical levels. The simplicity of the model makes it particularly helpful to derive dynamical insights on different aspects of monsoonal phenomena (e.g., Kasture et al. 1991; Krishnan and Kasture 1995; Sundaram et al. 2010; Choudhury and Krishnan 2011; Choudhury et al. 2018).

3 Circulation and Rainfall Diagnosis During ISM Breaks

Figure 1 shows composites of rainfall and 850 hPa horizontal winds, together with their corresponding anomaly maps, during ISM breaks based on the APHRODHITE land-only rainfall and ERA-Interim circulation products during 1979–2007. The ISM break days correspond to periods when the rainfall deficit of the standardised anomaly over central India (68°E–88°E and 18°N–28°N) is greater than 1 standard-deviation and should persist for at least 3 consecutive days or more (Rajeevan et al. 2010, Pai et al. 2016). There are a total of 25 (187) ISM break cases (days) during the period 1979–2007 (Table 1). The daily anomaly fields are constructed by subtracting the daily climatological mean values from the total fields. One can notice the extent of rainfall spanning from the CEH region to peninsular countries located over Southeast Asia during these periods (Fig. 1a), while there is deficient rainfall seen over the central part of India. Here, we also show the TRMM rainfall distribution during the break periods for the data available period from 1998 to 2014 to examine the spatial rainfall distribution over the land and oceanic region against the land-only rainfall distribution in APHRODITE data sets (Fig. 1b). We also have examined the break composites of rainfall using ERA-Interim data sets. It is seen that the ERA-Interim rainfall anomalies show increase of rainfall near the CEH foothills and decrease of rainfall over central India during ISM breaks (Figure S1 in supporting information). The pattern of rainfall anomalies is consistent among ERA-Interim, APHRODITE,
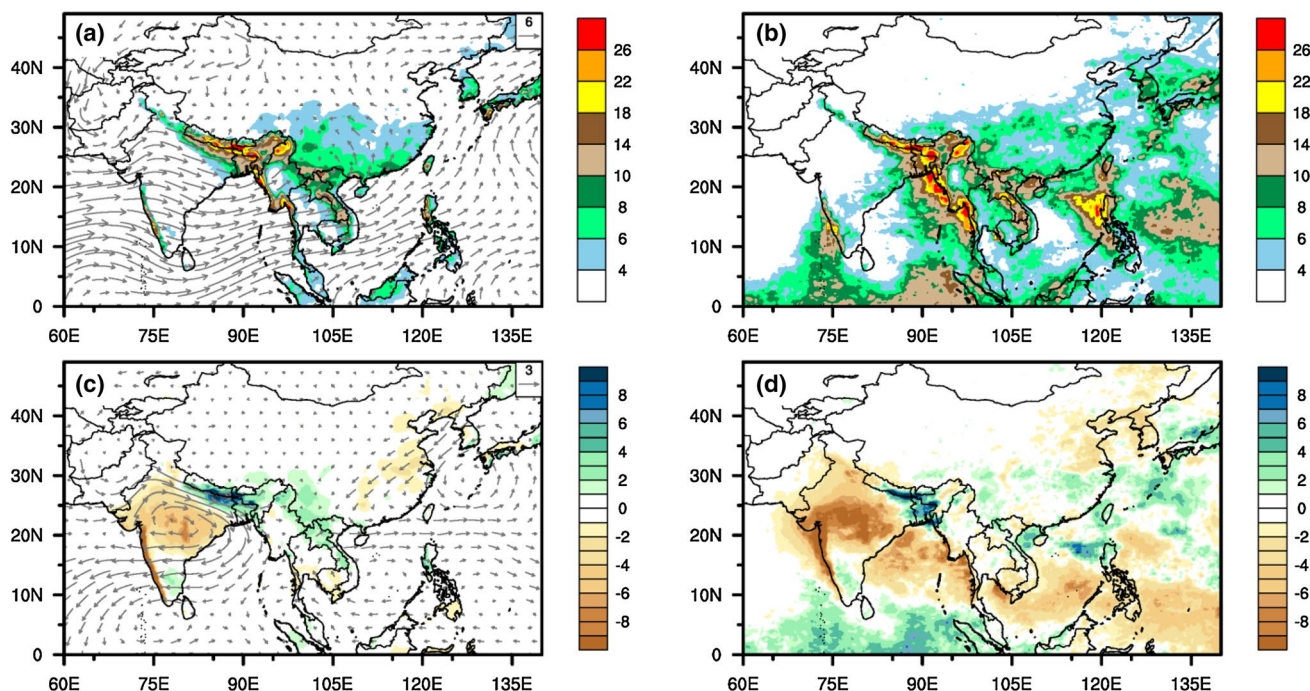
Fig. 1 **a**, **b** Composites of rainfall (shaded; mm day^{-1}) and 850 hPa winds (vector; m s^{-1}) and the corresponding anomalies **c**, **d** during the ISM break periods (Table 1). **a**, **c** uses rainfall from APHRO-and TRMM, although there are some differences in the magnitude of anomalies among the three data sets.

DITE for the break periods during 1979–2007 and **b**, **d** uses rainfall from TRMM for the break periods during 1998–2014. The winds are obtained from ERA-Interim reanalysis

A region of intense rainfall influenced by the Himalayan orography is generally prevalent over the Brahmaputra River Basin (encompassing the regions in the north-eastern parts of India, Tibet, Bhutan, Nepal, and Bangladesh) and coastal mountain ranges in Vietnam and Myanmar, and significant rainfall amounts are also noticeable over the oceanic regions of the eastern equatorial Indian Ocean and western North Pacific Ocean during the ISM break periods (Fig. 1b, d; see also Xie et al. 2006; Krishnamurthy and Shukla 2007; Vellore et al. 2014). The observed distribution of rainfall events during ISM break periods over the CEH foothills and the Indo-China region is positively skewed towards larger values as compared to active ISM periods (not shown). The 850 hPa wind field shows a low-level jet bypassing the peninsular part of India and also directed eastward towards Southeast Asia (Fig. 1a; see also Ramamurthy 1969; Krishnan et al. 2000), while anticyclonic circulation anomalies are noted in association with negative rainfall anomalies over the ISM-rainfed regions of central India (Fig. 1c). Positive rainfall anomalies during the break phase of ISM are mostly confined to the CEH foothill region (Fig. 1c), and various studies showed that these positive anomalies have associations with the migration of the monsoon trough to CEH foothill region (e.g., Raghavan 1973), moisture extraction by low-level southerlies from the Bay of Bengal (Medina

et al. 2010), maximisation of the synoptic-scale low-pressure anomaly over the Meghalaya Plateau (Romatschke and Houze 2011), and interaction of the equatorward advancing mid-latitude upper level westerly trough with ISM circulation (e.g., Ramamurthy 1969; Raghavan 1973; Vellore et al. 2014). Negative rainfall anomalies over the central part of India (Fig. 1c, d) are shown to have apparent associations with Rossby wave response induced by convectively stable anomalies seen over the Bay of Bengal (Krishnan et al. 2000), and also in part with westward propagating low-level circulation anomalies from the western North Pacific (Murata et al. 2017). The circulation anomalies seen over East Asia (Fig. 1c) show slight similarities to the Pacific-Japan pattern (Nitta 1987), and the corresponding phase of rainfall anomaly pattern bears resemblance with the ''southern flood-northern drought'' pattern over China (Wang 2002; Yu et al. 2004).

3.1 Latent Heating and Mid-tropospheric Circulation

Figure 2a shows the composites of column-mean diabatic heating rates for the ISM break periods (Table 1). The corresponding diabatic heating anomalies during the ISM break are shown in Fig. 2b. The diabatic heating estimation follows the procedure described in Yanai et al. (1973) with most of the diabatic heating coming from LH release.
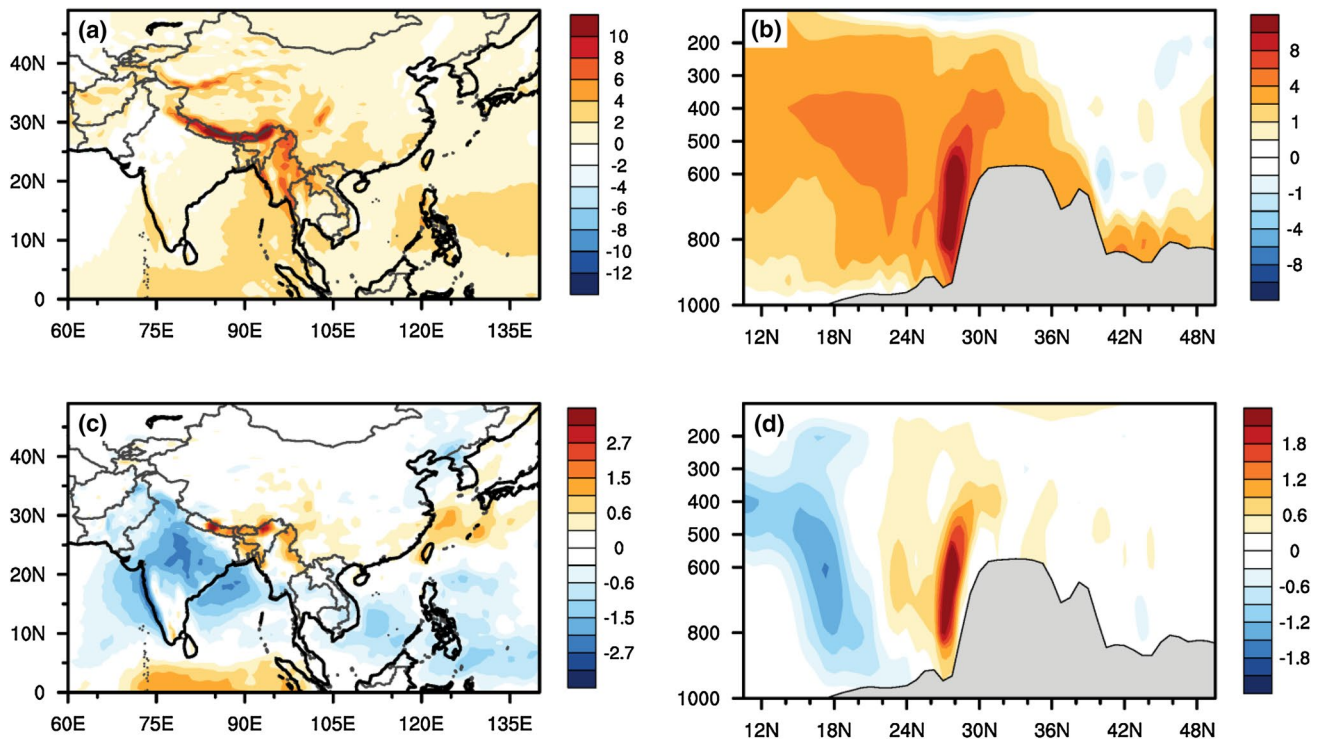
Fig. 2 **a**, **c** Composites of column-mean diabatic heating (K day^{-1}) and its anomaly during the ISM break periods (see Table 1). The diabatic heating is diagnosed using ERA-Interim reanalysis following the procedure described in Yanai et al. (1973). **b**, **d** Composites of latitude-pressure cross-section of diabatic heating and its anomaly (shaded; K day^{-1}) averaged across the Tibetan Plateau (85°E–105°E) during ISM breaks. The grey shaded region in **b**, **d** represents the topography

The total heating during ISM breaks is pronounced over the CEH and Indo-China peninsular countries and the equatorial eastern Indian Ocean, while the heating over the central and northern parts of India is minimal (Fig. 2a). A latitude-pressure cross-section of heating averaged over the longitudes 85°E–105°E shows pronounced condensational LH (10 K day^{-1} or more) over the CEH foothill region extending up to 400 hPa together with significant heating over the northern Bay of Bengal (Fig. 2b). Positive heating anomalies are evident over the CEH foothills and negative heating anomalies over central India (Fig. 2c), which are consistent with the pattern of rainfall anomalies. The anomalous heating is more pronounced near the CEH foothills, with noticeable magnitudes over the equatorial Indian Ocean and China Sea (Fig. 2d). Also notice that anomalous heating during ISM breaks is particularly confined to the CEH foothill region, so that the sharp vertical heating gradient can serve as a source of cyclonic vorticity (e.g., Kennett and Toumi 2005). Vellore et al. (2014) reported a twofold increase in precipitation over the CEH foothills during ISM breaks as compared to active monsoon periods, and this feature is also consistent with the LH anomalies seen across the CEH foothill region (not shown).

Figure 3 shows the composites of mid-tropospheric wind and geopotential height, and their corresponding anomalies,

during the ISM break periods (Table 1). The wind field during ISM breaks shows northwesterlies intruding into the Indian subcontinent in the upstream environment of the southward advancing westerly trough, and anticyclonic circulation environment over the Arabian Peninsula and northwest Pacific (Fig. 3a). Anomalous heights during ISM breaks reveal a signature of a poleward extending meridionally oriented pattern of alternating anticyclonic and cyclonic anomalies extending from the Indian subcontinent to the high latitudes (Fig. 3b). Note that the regions of anticyclonic (cyclonic) anomalies over the Indian subcontinent (Asian mid-latitude belt) exceed the 95% confidence level. Emergence of the poleward extending alternating pattern of circulation anomalies (Fig. 3b) bears resemblance of meridionally dispersing Rossby waves forced by anomalous heating over the tropics/monsoon areas as noted in earlier studies (e.g., Sardeshmukh and Hoskins 1988; Sato and Kimura 2005; Krishnan et al. 2009). Hoskins and Karoly (1981) demonstrated that vorticity sources in the tropics and subtropics tend to generate wave trains with long wavelengths that can propagate poleward to the middle and high latitudes. In particular, they noted that vorticity forcing located in the subtropics is effective in setting up poleward extending meridional wave trains. In addition, they showed, based on theoretical considerations, that the meridional wave train

(a)

(b)
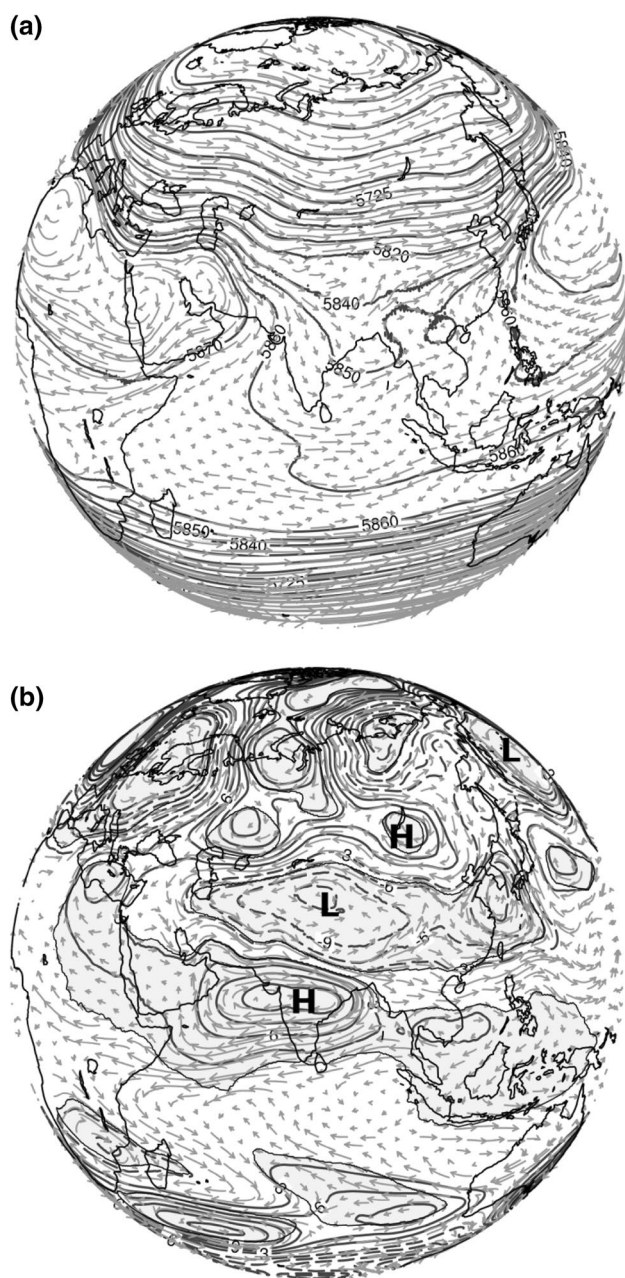
Fig. 3 Composites of **a** total mid-tropospheric geopotential height (solid contour; m) and horizontal winds (vector; m s^{-1}); **b** the associated anomalous fields during the ISM break periods (see Table 1). The grey shaded region in **b** represents statistical level (1%) of significance using the standard t test procedure

patterns can be explained in terms of Rossby wave dispersion in a barotropic atmosphere. In an another study, Lim and Chang (1983) suggested that the vertical shear of mean zonal flow plays an important role in the meridional propagation of wave disturbances generated by tropical heating.

We performed a similar analysis to examine the large-scale circulation response during active ISM (Figure S2 in supporting information). The appearance of a meridionally

extending pattern of circulation anomalies is also noted for the active ISM. While the polarity of circulation anomalies over the Indian subcontinent is opposite to that of the ISM break, it is noticed that poleward extending wave train for the active ISM is mostly located near the longitudinal band over East Asia and West Pacific. Also the spatial scale of the meridional wave-train anomalies appears to be relatively smaller during the active ISM conditions. This suggests that the generation of poleward extending meridional wave train is generic to the anomalous heating over the subtropical latitude belt, although the longitudinal band of the wave train may depend on the location of the forcing. In a more recent study, Krishnamurti et al. (2015) have proposed a monsoonal connection to the rapid Arctic ice melt since the mid-2000s through transport of atmospheric heat fluxes from the monsoon belt to the Arctic. They hypothesised that increased atmospheric heat content associated with heavy rainfall over northwest India and Pakistan is transported by upper level anticyclonic outflows from the South Asian monsoon region towards the mid-latitudes and the Canadian Arctic through a meridional wave train.

3.2 Anomalous Evolution of Heating and Circulation

The spatio-temporal evolution of the diabatic heating and mid-tropospheric circulation anomalies is examined here through the use of a lead–lag analysis for the ISM break periods, as shown in Table 1. Figure 4 shows the lead–lag plots of vertically averaged diabatic heating anomalies and 500 hPa wind and geopotential height anomalies for 9 days starting from lag −5 up to lag +3, where lag 0 corresponds to the day of commencement of the ISM break (see Table 1). There is generally a good correspondence in the lag–lead patterns of precipitation and diabatic heating anomalies, which clearly suggests that heating anomalies are mostly related to precipitation variations and associated LH release—which is consistent with the analysis of Hazra and Krishnamurthy (2015) who pointed out coherent links among precipitation, diabatic heating, and circulation anomalies over the Indian subcontinent on intra-seasonal timescales. It is seen that 500 hPa height excess is substantial over the Indian subcontinent from lag −2 to lag +3 (Fig. 4d, i), and negative heating anomalies over the Indian subcontinent are co-located with anticyclonic circulation anomalies during this period. The spatial scale of this anticyclonic anomaly can be seen extending from the western Arabian Sea to the tropical western Pacific, across the Indian subcontinent. Another notable feature during the ISM break period is a large-scale mid-tropospheric cyclonic anomaly spanning over the mid-latitude regions of the Asian continent during this period. It is interesting to note that the southern flank of the aforesaid Asian continental mid-tropospheric cyclonic

circulation (ACMCC) is accompanied by positive heating anomalies that extend from the CEH foothills towards southeast China. While significant cyclonic circulation anomalies are distinct over northeast China, Korea, and Japan between lag −5 and lag −3 (Fig. 4a–c), a larger spatial extent of more pronounced cyclonic (anticyclonic) anomalies over the Asian mid-latitudes (south and southeast Asia) is subsequently noticed between lag −2 and lag +3 (Fig. 4d–i).

The emerging point for our discussion here is the southwest–northeast-oriented anomalous meridional wave train at 500 hPa level consisting of alternating mass excess and deficits from the Asian monsoon region extending poleward into the high latitudes during ISM break periods (Fig. 4). A question arises on the associated direction/causality: Does the anomalous build-up of heat sources and sinks over the Indian subcontinent and Indo-China region during ISM break periods play a role in promoting the ACMCC?. We address this by conducting a suite of numerical sensitivity experiments using a simplified global atmospheric general circulation model (GCM) forced with observed heating.

4 Thermally Forced Atmospheric Circulation Response During ISM Breaks

The simplified atmospheric GCM is integrated into a forced-damped mode for steady-state solutions. Five experiments (CTRL, EXP1, EXP2, EXP3, and EXP4) are conducted which essentially differ in terms of LH prescription. Initial conditions correspond to a resting atmosphere and temperatures at different vertical levels are set to their global mean values in all experiments (see Choudhury and Krishnan 2011). The model also employs linear damping in the form of Rayleigh friction (in vorticity and divergence equations) and Newtonian cooling (in thermodynamic equation), and both are set to have an e-folding decay time-scale of 5 days. The model is integrated for 100 days with fixed heating and damping terms to obtain steady-state solutions.

The forcing for the control experiment (CTRL) is the three-dimensional climatological mean heating for the June–September (JJAS) monsoon season, and the LH is constructed from the TRMM PR 3A25 monthly surface rain estimates and vertical profiles of stratiform and convective precipitation following the algorithm of Schumacher et al. (2004). The ERA-Interim heating in Fig. 2 basically corresponds to the diabatic heating field. Given that LH is the dominant component of diabatic heating associated with precipitation variations over the tropics and monsoonal areas (e.g., Yanai and Tomita, 1998), we have employed the TRMM-based LH fields to force the model. The details of constructing the JJAS climatological mean LH are described in Choudhury and Krishnan (2011) and Choudhury et al. (2018). Figure 5 shows the column-mean JJAS climatology

of LH and the simulated mid-level (in model corresponds to $\sigma = 0.58$–0.42) circulation. The climatological mean summer monsoon heat source distinctly exhibits LH maxima over the northern Bay of Bengal, Myanmar coast, and the west coast of India (Fig. 5a). The associated mid-level circulation response shows a large-scale cyclonic circulation zonally extending from the western Arabian Sea eastward into the Indian subcontinent, Bay of Bengal, Southeast Asia, and the tropical West Pacific, and meridionally extending between 10°N and 30°N. The zonal scale of the simulated mid-level cyclonic circulation is approximately about 8000 km.

After obtaining the steady-state circulation response to the climatological mean LH, four sensitivity experiments (EXP1, EXP2, EXP3, and EXP4) have been conducted wherein the large-scale atmospheric response to anomalous heat sources/sinks during ISM breaks is examined. In EXP1, the model is forced by the total LH constructed by superposing the three-dimensional climatological mean heating and the LH anomaly specified over a large region 45°E–145°E; 15°S–40°N (referred in the text as the Asian monsoon domain). The three-dimensional LH anomaly field in EXP1 is extracted from the observed TRMM 3B42 precipitation anomalies over the Asian monsoon domain and then combined with the normalised heating profiles derived from the Schumacher et al. (2004) algorithm. The stratiform and convective rain fractions over the region of the precipitation anomaly are set to their corresponding climatological mean values, so that the vertical structure of the imposed LH anomaly at any given grid point is the same as that of the climatological profile. The column-mean heating anomaly in EXP1 shows positive anomalies over the CEH foothills zonally extending up to eastern China and over the equatorial eastern Indian Ocean, whereas negative anomalies are seen over the Indian region (west coast and central India), Bay of Bengal, Southeast Asia, and South China sea (Fig. 6a). The large-scale pattern of anomalous heat sources/sinks in EXP1 is consistent with the pattern of anomalous convection during ISM breaks over the Asian monsoon region (e.g., Krishnan et al. 2000). The second sensitivity experiment (EXP2) is similar to EXP1, except that the anomalous heating is located over the regions covering Southeast and East Asia (104°E–140°E; 12°N–38°N, Fig. 6b). In the third sensitivity experiment (EXP3), the circulation response is examined with respect to the heating anomaly confined over the CEH foothills and Indo-China (dotted region shown in Fig. 6c). Finally, the circulation response is examined with respect to only the heating anomaly over central India and the CEH foothills including the Indo-China region (dotted region in Fig. 6d) in the fourth experiment EXP4.
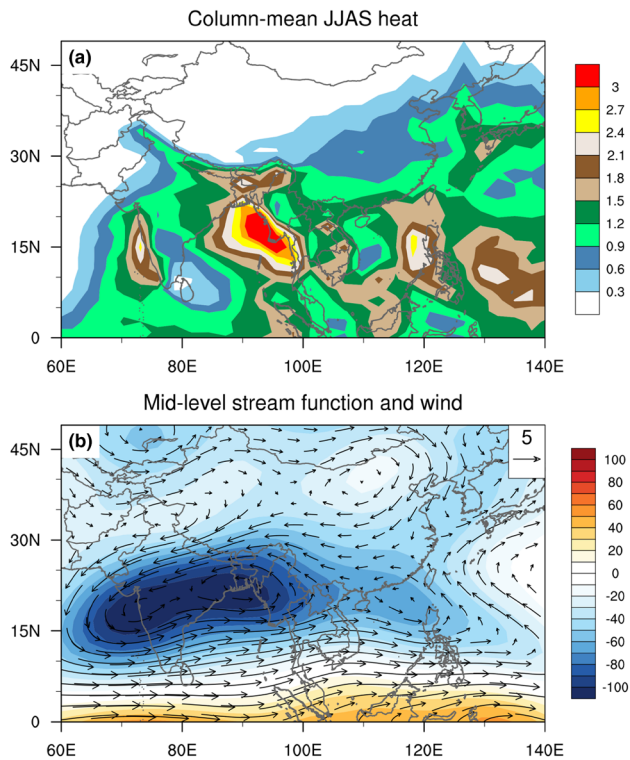
Figure 7 shows the anomalous mid-level circulation response to the imposed heating anomalies from the four experiments EXP1, EXP2, EXP3, and EXP4. The anomalous circulation is constructed by taking the difference in
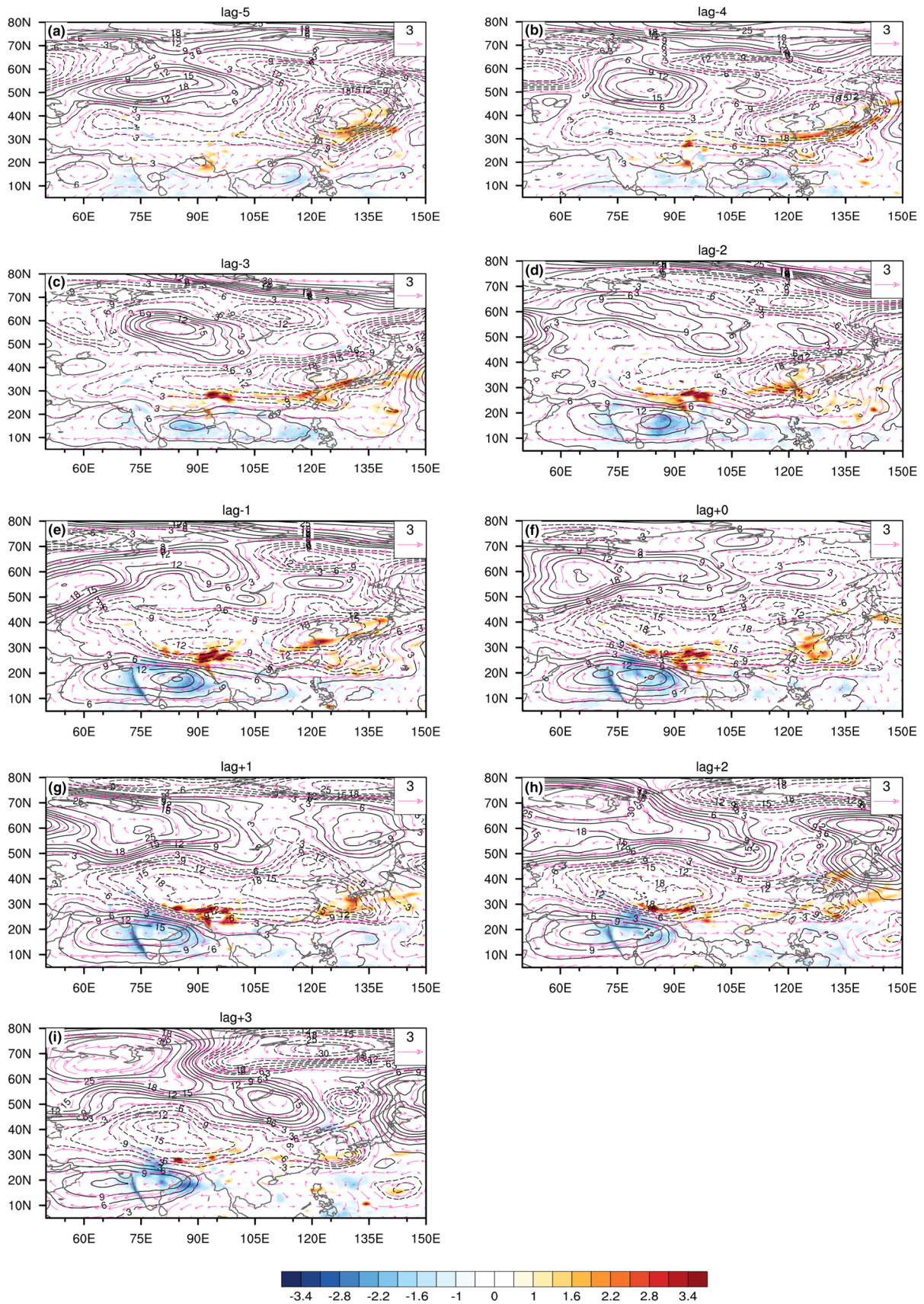
Fig. 5 **a** Column-mean climatological JJAS (June–September) LH (K day^{-1}) derived from the TRMM PR 3A25 monthly rainfall products which is used to force the GCM. **b** The GCM simulated mid-level stream function (ψ) (shaded; ×10^{-5} m^2 s^{-1}) and the horizontal winds (m s^{-1}) in response to the climatological LH shown in **a**

each of the four sensitivity experiments with respect to the CTRL experiment. The meridional wave train composed of alternating anticyclonic and cyclonic anomalies is broadly captured in EXP1 (Fig. 7a). This poleward extending wave train shows a prominent anticyclonic anomaly over the Indian subcontinent and the Middle Eastern countries, a cyclonic anomaly further north of the Himalayas extending over the mid-latitude region of the Tibetan Plateau, central–eastern China (ACMCC), together with an anticyclonic anomaly over northern Eurasia, followed by a cyclonic anomaly further north. Also seen in Fig. 7a is a cyclonic anomaly over the equatorial central–eastern Indian Ocean in association with enhanced near-equatorial convection during ISM breaks (Krishnan et al. 2000, 2006). The simulated anticyclonic anomaly over the Indian subcontinent in Fig. 7a shows a westward displacement with relatively

high amplitudes over the Middle East as compared to the observed anomaly during ISM breaks. While recognising these differences in the simulated and observed pattern of circulation anomalies, EXP1 clearly captures the overall large-scale structure of the poleward extending meridional wave train in the mid-levels during ISM breaks. The mid-level anomalous response in EXP2 shows an anticyclonic anomaly over the Indian region and a cyclonic anomaly over central–eastern China (Fig. 7b). The positive heating anomalies in EXP2 are confined over the southeast and eastern China (Fig. 6b). Although EXP2 shows signatures of the meridional wave train (Fig. 7b), the magnitude of the circulation anomalies is relatively weak as compared to EXP1. The anomalous circulation response in EXP3, forced with an anomalous heat source over the CEH foothills and heat sink over the Indian landmass, is shown in Fig. 7c. In this case, we see a clearer meridional wave train of alternating anticyclonic and cyclonic anomalies extending from the Indian subcontinent into the middle and higher latitudes. Finally, in EXP4, which includes positive heating anomalies over the CEH foothills (as like in EXP3) and negative heating anomalies over the Indian landmass, the anomalous meridional circulation response is further amplified with a poleward extending pattern of alternating high and low clearly evident (Fig. 7d). From Fig. 7c, d, it is evident that the circulation response to the north of CEH foothills appears to be more sensitive to the anomalous heat source over the CEH foothills and the Indo-China region.

In short, the results from the four sensitivity experiments indicate that the large-scale forced response to positive LH anomalies over the CEH foothills, Indo-China, and central–eastern China and negative anomalies over the Indian subcontinent has potential consequences to the observed poleward extending meridional wave train in the mid-tropospheric levels during ISM breaks. In particular, the meridional wave-train pattern including the anomalous high over the Indian landmass appears to be due to the combined effects of the anomalous heat source over the CEH foothills and the Indo-China region, and the anomalous heat sink over the Indian landmass during ISM breaks. On the other hand, the anomalous LH over central–eastern China associated with ACMCC during ISM breaks tends to enhance the magnitude and spatial extent of the mid-latitude cyclonic anomaly over central–eastern China.

5 Implications of Mid-tropospheric Circulation Anomaly for Heavy Precipitation

Regions in the vicinity of Indo-China and near the Sichuan basin of China often experience extreme precipitation and floods during the summer monsoon season (Fan et al. 2015;
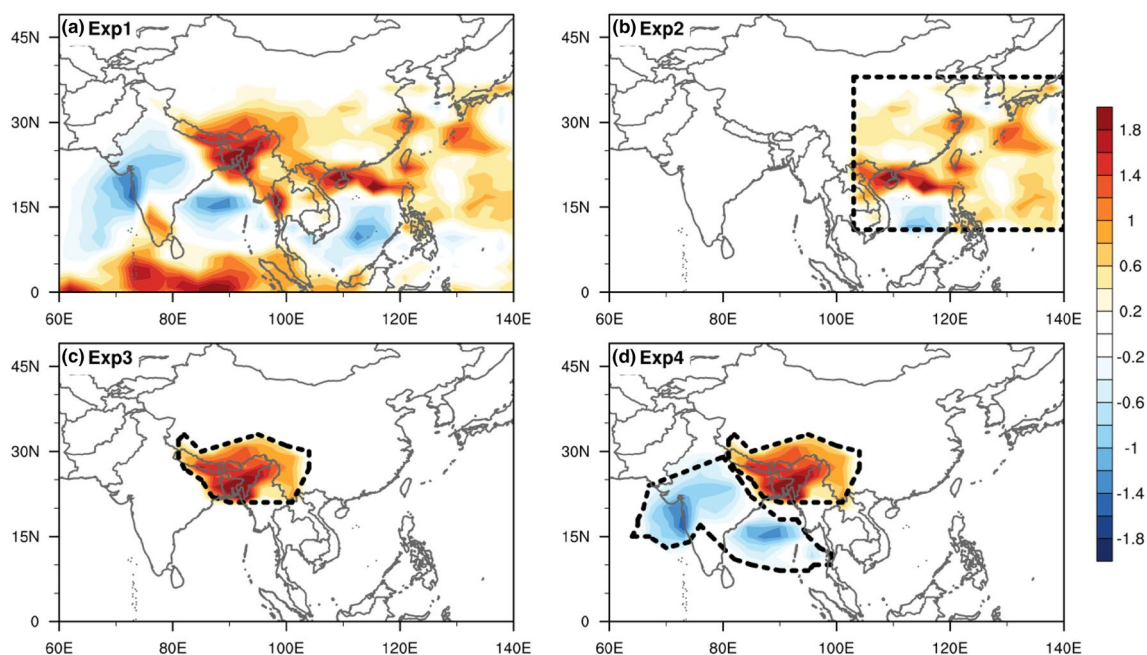
Fig. 6 GCM experiments with LH anomalies over the region **a** ISM domain (45°E–145°E; 15°S–40°N) in EXP1 **b** Southeast and East Asia (104°E–140°E; 12°N–38°N) in EXP2, **c** CEH foothills and the adjoining areas of Indo-China region (black dashed line) in EXP3, and **d** Indian subcontinent along with the CEH foothills and the adjoining areas of Indo-China region (black dashed line). The LH anomalies represent the deviations of LH estimated over the specified region in EXP1, EXP2, EXP3, and EXP4 during ISM breaks with that of the climatology of LH (Fig. 5a) in CTRL experiment

Kim et al. 2019). Vellore et al. (2014) reported that the intensification of mid-tropospheric cyclonic vorticity and upward motions over the CEH foothills, during ISM breaks, tends to promote deep convection and localised heavy rainfall. They further indicated, based on high-resolution regional climate model simulations, that heavy precipitation over the CEH foothills can increase twofold during ISM breaks as compared to active ISM periods.

Here, we examine the implications of the ACMCC anomaly pattern on heavy precipitation over the Indo-China region (inset in Fig. 8) using the daily observed precipitation from the APHRODITE dataset for the period 1979–2007. It can be noticed from Fig. 1c that the Indo-China domain, which includes the CEH foothills, experiences above normal precipitation during ISM breaks. To distinguish the role of ACMCC, we bring out the comparison between the break and active periods as the active periods lack the ACMCC pattern. Figure 8a shows the box–whisker plot of the count of heavy rainfall grids over the Indo-China domain. For this purpose, we first obtain the 95th and 99th percentile thresholds at each grid point in the domain using the daily rainfall for the July and August months during 1979–2007. To determine A95 and A99, we count at each grid point of the Indo-China domain the number of times the July and August rainfall for the active ISM periods exceeds the 95th and 99th

percentile threshold, respectively. It must be mentioned that the A95 and A99 counts are determined for each of the 16 active ISM cases individually, which yields 16 values of A95 and 16 values of A99, respectively. Also, the A95 and A99 counts are computed separately for days from lag −2 to lag +3 (total 6 days). The same approach is applied for the ISM break periods to determine the 25 values of B95 and B99. From Fig. 8a, it can be noticed that the median counts of B95 and B99 are 225 and 28, respectively, which are more than twice as compared to the corresponding counts for the active periods A95 (110) and A99 (10). Furthermore, the upper tail of the counts is substantially higher for B95 and B99, indicating the large variability of extreme rainfall occurrences during ISM breaks as compared to ISM active periods.

Composites of total rainfall averaged over the Indo-China domain from lag −6 to lag +6 are shown in Fig. 8b for the ISM active and break cases. A distinctive increase in the total precipitation during ISM breaks is evident, as compared to the ISM active cases, for lag −2 to lag +3 over the Indo-China region. Our understanding suggests that the mid-tropospheric circulation anomaly over China and East Asia, associated with the ACMCC pattern during ISM breaks, can act as an envelope of large-scale cyclonic vorticity that can in turn facilitate the growth of deep convective

Fig. 7 The mid-level circulation (m s^{-1}) and geopotential height (m) anomalies in response to LH anomalies shown in Fig. 6 in all the experiments EXP1, EXP2, EXP3, and EXP4. The circulation and height anomalies in each experiment (**a–d**) represent the corresponding deviations from the mean circulation and height fields in CTRL experiment

(a) EXP1 (b) EXP2 (c) EXP3 (d) EXP4

-32 -16 -8 -4 -2 -1 1 2 4 8 16 32
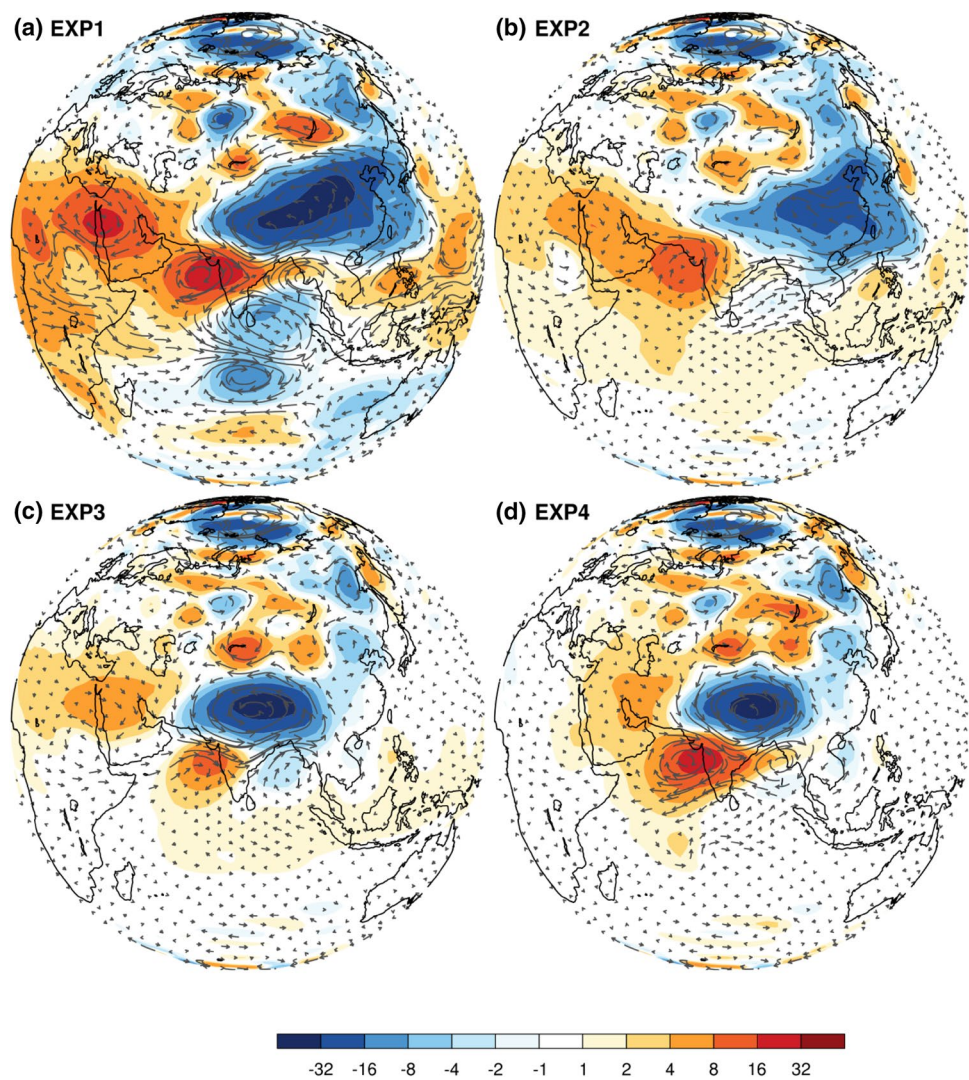
systems and heavy precipitation over the southern flanks of the ACMCC. Basically, the large-scale circulation anomaly to the east of the Tibetan Plateau during ISM breaks corresponds to dispersing downstream Rossby waves which are triggered by anomalous heating over the Indian subcontinent and the Himalayan foothills (Krishnan et al. 2009). Furthermore, precipitation enhancement over the eastern side of the Tibetan Plateau is usually associated with eastward propagating synoptic-scale troughs embedded in the subtropical westerly flow (Vellore et al. 2014). As the subtropical westerlies move towards the lower latitudes during ISM breaks, they tend to produce heavy rains over the CEH foothills and the adjoining areas of Indo-China in association with strong 500 hPa convergence of moisture transported from the Bay of Bengal towards the CEH foothills, together with additional contributions from mesoscale orographic effects which tend to amplify the vertical motions in the region (Vellore et al. 2014). In summary, the increase in the frequency of heavy precipitation occurrences over the

Indo-China region during ISM breaks is a multi-scale interactive process and supported by the background large-scale cyclonic vorticity associated with the ACMCC anomaly pattern.

6 Summary

The Asian summer monsoon heating is known to force summer-time descent over the Mediterranean and Sahara regions through westward extending stationary Rossby waves (Rodwell and Hoskins 1996; Liu et al. 2001). Several researchers have investigated the large-scale extra-tropical circulation response to monsoon heating on seasonal and inter-annual time-scales (Lau et al. 2000; Wang et al. 2001; Wu 2002; Wu and Wang 2002; Ding and Wang 2005; Saeed et al. 2011b). On the other hand, the role of ISM subseasonal variations on the large-scale circulation response over the extra-tropics is a topic that needs adequate investigations. An intriguing

(a)

(b)
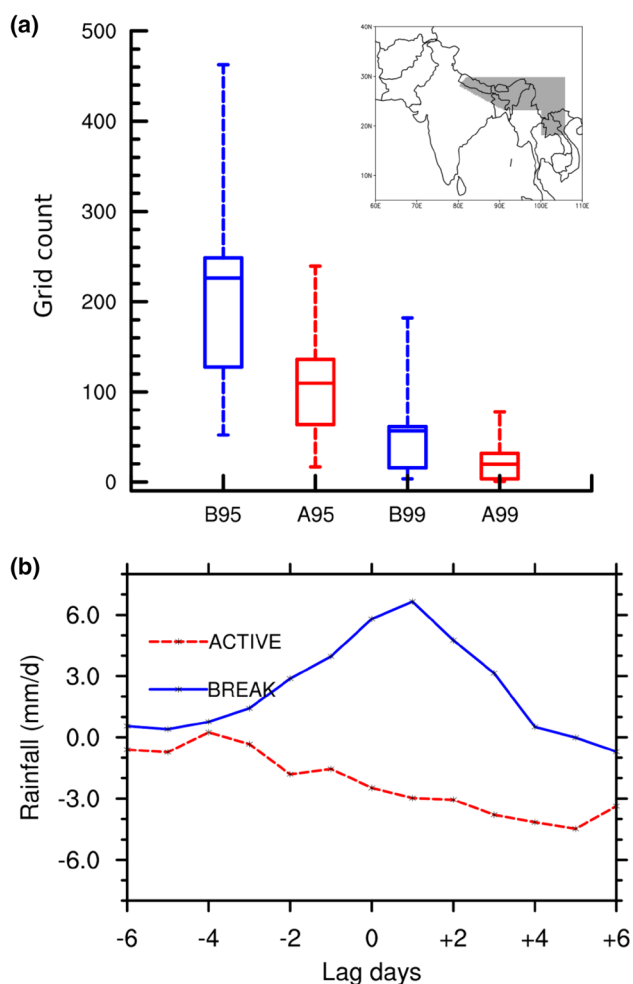
Fig. 8 a Box–whisker plot of count of heavy rainfall grids in APH-RODITE rainfall data diagnosed from the Indo-China region shown in the inset. The heavy rainfall counts for the active (A95 and A99) and break (B95 and B99) ISM periods are estimated using the 95th and 99th percentile of daily rainfall threshold at each grid point (derived from July and August daily rainfall during 1979–2007). The total number of grid points in the Indo-China region is 2924. **b** The lead–lag evolution of area averaged rainfall anomalies over the Indo-China region (inset) from lag −6 to lag +6 days

feature during the ISM break periods is the formation of a mid-tropospheric continental-scale cyclonic circulation anomaly extending over the Asian mid-latitudes (as referred ACMCC in the text). While studies have reported that equatorward advancing large-amplitude troughs in the mid-latitude westerlies can induce ISM breaks (e.g., Ramaswamy 1962; Krishnan et al. 2000), the influence of latent heating anomalies over the Indian landmass and the CEH foothills on the large-scale extra-tropical circulation response is not well understood.

By performing detailed diagnostic analyses using observed data sets and reanalysis products, the present study provides a mechanistic understanding of the

ACMCC pattern. Our results indicate that the ACMCC is part of a larger pattern of meridionally dispersing Rossby waves that extends from the tropics into higher latitudes during ISM breaks. It is further noted that the aforesaid large-scale meridional circulation pattern during ISM breaks is largely forced by LH anomalies over central-north India and the CEH foothills. Model experiments reproduce the meridional circulation pattern when forced by the ISM break pattern of increased LH over the CEH foothills and decreased LH over the plains of central-north India. While the enhancement of LH over the CEH foothills is found to be critical for the formation of the mid-tropospheric cyclonic anomaly around the Tibetan Plateau, the large-scale meridional pattern across the Asian continent is fostered by the north–south dipolar pattern of the LH anomaly over the Indian subcontinent. Our analysis further suggests that the mid-tropospheric circulation anomaly over China and East Asia associated with the ACMCC pattern facilitates the growth of deep convective systems and heavy precipitation over the southern flanks of the ACMCC. It is noted that the frequency of extreme rainfall occurrences over Indo-China shows a twofold increase during ISM break periods as compared to active ISM conditions. The enhanced frequency of heavy precipitation occurrences over the Indo-China region during ISM breaks involves the combined effects of eastward propagating synoptic-scale troughs in the subtropical westerlies, strong mid-level convergence of moisture transport from the Bay of Bengal, and mesoscale orographic effects (Vellore et al. 2014), supported by the background large-scale cyclonic vorticity associated with the ACMCC anomaly pattern.

In a recent study, Krishnamurti et al. (2015) have proposed that poleward transport of LH release from intense precipitation events over the northwestern part of India and Pakistan through meridional wave trains can reach as far as Canadian Arctic, resulting in accelerating the melting of Arctic sea ice. From a climate change point of view, this implies that changes in the frequency and intensity of ISM breaks and associated heating anomalies over the ISM and adjoining areas can potentially exert far reaching impacts over the Arctic region. There are significant uncertainties in the CMIP5 model projections of the northward propagating low-frequency intra-seasonal modes associated with the ISM active and break phases (Sharmila et al. 2015), thus warranting further research in this area.

GOTHAM, Sacre-X and CoSy-CC2. The data providers of all used observational precipitation data sets (IMD, APHRODITE, and TRMM) and the ECMWF reanalysis (ERA-Interim) circulation products are thankfully acknowledged. The model computations were performed on the IITM high-performance computing (HPC) facility at IITM.

Compliance with Ethical Standards

References

Annamalai H, Slingo JM (2001) Active/break cycles: diagnosis of the intraseasonal variability of the Asian summer monsoon. Clim Dyn 18:85–102

Bourke W (1974) A multi-level spectral model I. Formulation and hemispheric integrations. Mon Weather Rev 102:687–701

Choudhury AD, Krishnan R (2011) Dynamical response of the South Asian monsoon to latent heating from stratiform and convective precipitation. J Atmos Sci 68:1347–1363

Choudhury AD, Krishnan R, Ramarao MVS, Vellore R, Singh M, Mapes B (2018) A phenomenological paradigm for midtropospheric cyclogenesis in the Indian summer monsoon. J Atmos Sci 75:2931–2954

Dee DP et al (2011) The ERA-interim reanalysis: configuration and performance of the data assimilation system. Quart J R Meteorol Soc 137:553–597

Dhar ON, Nandargi S (2000) A study of floods in the Brahmaputra Basin in India. Int J Climatol 20:771–781

Dhar ON, Soman MK, Mulye SS (1984) Rainfall over the southern slopes of the Himalayas and the adjoining plains during breaks in the monsoon. J Climatol 4:671–676

Ding Q, Wang B (2005) Circumglobal teleconnection in the Northern Hemisphere summer. J Clim 18:3483–3505

Ding Q, Wang B (2007) Intraseasonal teleconnection between the summer Eurasian wave train and the Indian monsoon. J Clim 20:3751–3767

Ding Q, Wang B (2009) Predicting extreme phases of the Indian summer monsoon. J Clim 22:346–363

Enomoto T, Hoskins BJ, Matsuda Y (2003) The formation mechanism of the Bonin high in August. Q J R Meteorol Soc 129:157–178

Fan J, Rosenfeld D, Yang Y, Zhao C, Leung LR, Li Z (2015) Substantial contribution of anthropogenic air pollution to catastrophic floods in Southwest China. Geophys Res Lett 42:6066–6075

Gadgil S, Joseph PV (2003) On breaks of the Indian monsoon. Proc Indian Acad Sci Earth Planet Sci 112:529–558

Hazra A, Krishnamurthy V (2015) Space-time structure of diabatic heating in monsoon intraseasonal oscillation. J Clim 28:2234–2255

Hoskins BJ, Karoly DJ (1981) The steady linear response of a spherical atmosphere to thermal and orographic forcing. J Atmos Sci 38:1179–1196

Houze RA (1997) Stratiform precipitation in regions of convection: a meteorological paradox? Bull Am Meteorol Soc 78:2179–2196

Houze RA, Wilton DC, Smull BF (2007) Monsoon convection in the Himalayan region as seen by the TRMM Precipitation radar. Q J R Meteorol Soc 133:1389–1411

Huffman GJ, Adler RF, Rudolf B, Schneider U, Keehn PR (1995) Global precipitation estimates based on a technique for combining satellite-based estimates, rain gauge analysis, and NWP model precipitation information. J Clim 8:1284–1295

Huffman G, Adler R, Arkin P, Chang A, Ferraro R, Gruber R, Janowiak J, McNab A, Rudolf B, Schneider U (1997) The global precipitation climatology project (GPCP) combined precipitation data set. Bull Am Meteor Soc 78:5–20

Kasture SV, Satyan V, Keshavamurty RN (1991) A model study of the 30–50 day oscillation in the tropical atmosphere. Mausam 42:241–248

Kennett EJ, Toumi R (2005) Himalayan rainfall and vorticity generation within the Indian summer monsoon. Geophys Res Lett 34:L04802

Keshavamurthi RN, Awade ST (1974) Energy conversions during weak monsoon. Research Report Indian Institute of Tropical Meteorology RR-015, pp 224–231

Kim I-W, Oh J, Woo S, Kripalani RH (2019) Evaluation of precipitation extremes over the Asian domain: observation and modelling studies. Clim Dyn 52:1317–1342. https://doi.org/10.1007/s00382-018-4193-4

Kripalani RH, Kulkarni A, Singh SV (1997) Association of the Indian summer monsoon with the Northern Hemisphere midlatitude circulation. Int J Climatol 17:1055–1067

Krishnamurthy V, Kinter JL III (2003) The Indian monsoon and its relation to global climate variability. In: Rodó X, Comín FA (eds) global climate. Springer, Berlin, pp 186–236

Krishnamurthy V, Shukla J (2007) Intraseasonal and seasonally persisting patterns of Indian monsoon rainfall. J Clim 20:3–20

Krishnamurti TN, Bedi HS, Subramaniam M (1989) The summer monsoon of 1987. J Clim 2:321–340

Krishnamurti TN, Chakraborty A, Mishra AK (2010) Improving multimodel forecasts of the vertical distribution of heating using the TRMM profiles. J Clim 23:1079–1094

Krishnamurti TN, Krishnamurti R, Das S, Kumar V, Jayakumar A, Simon A (2015) A pathway connecting monsoonal heating to rapid Arctic ice melt. J Atmos Sci 72:5–34

Krishnan R, Kasture SV (1995) Sensitivity of the tropical nonlinear stationary Kelvin and Rossby waves to the vertical structure of heating. Proc Indian Acad Sci 104:579–606

Krishnan R, Sugi M (2001) Baiu rainfall variability and associated monsoon teleconnection. J Met Soc Jap 79:851–860

Krishnan R, Zhang C, Sugi M (2000) Dynamics of breaks in the Indian summer monsoon. J Atmos Sci 57:1354–1372

Krishnan R, Ramesh KV, Samala BK, Meyers G, Slingo JM, Fennessy MJ (2006) Indian Ocean–monsoon coupled interactions and impending monsoon droughts. Geophys Res Lett 33:L08711

Krishnan R, Kumar V, Sugi M, Yoshimura J (2009) Internal feedbacks from monsoon–mid-latitude interactions during droughts in the Indian summer monsoon. J Atmos Sci 66:553–578

Lau KM, Kim KK, Yang S (2000) Dynamical and boundary forcing characteristics of regional components of the Asian Summer Monsoon. J Clim 13:2461–2482

Lim H, Chang C-P (1983) Dynamics of teleconnections and Walker circulations forced by equatorial heating. J Atmos Sci 40:1897–1915

Liu YM, Wu GX, Liu H, Liu P (2001) Condensation heating of the Asian summer monsoon and the subtropical anticyclone in Eastern Hemisphere. Clim Dyn 17:327–338

Medina S, Houze R Jr, Kumar A, Niyogi D (2010) Summer monsoon convection in the Himalayan region: terrain and land cover effects. Q J R Meteorol Soc 136:593–616

Murata F, Terao T, Fujinami H et al (2017) Dominant synoptic disturbance in the extreme rainfall at Cherrapunji, Northeast India, based on 104 years of rainfall data (1902–2005). J Clim 30:8237–8251

Nitta T (1987) Convective activities in the tropical western Pacific and their impact on the Northern Hemisphere summer circulation. J Meteorol Soc Jpn 65:373–390

Pai DS, Sridhar L, Rajeevan M, Sreejith OP, Satbhai NS, Mukhopadhyay B (2014) Development of a new high spatial resolution (0.25° × 0.25°) long period (1901–2010) daily gridded rainfall data set over India and its comparison with existing data sets over the region. MAUSAM 65:1–18

Pai DS, Sridhar L, Ramesh Kumar MR (2016) Active and break events of Indian summer monsoon during 1901–2014. Clim Dyn 46:3921–3939

Raghavan K (1973) Break-monsoon over India. Mon Weather Rev 101:33–43

Rajeevan M, Gadgil S, Bhate J (2010) Active and break spells of the Indian summer monsoon. J Earth Syst Sci 119:229–247

Ramamurthy K (1969) Monsoon of India: some aspects of the 'break' in the Indian southwest monsoon during July and August. Forecasting manual 1-57 no. IV 18.3. India Meteorological Department, Poona, India

Raman CRV, Rao YP (1981) Blocking highs over Asia and monsoon droughts over India. Nature 289:271–273

Ramaswamy C (1962) Breaks in the Indian summer monsoon as a phenomenon of interaction between the easterly and the sub-tropical westerly jet streams. Tellus 14:337–349

Ramesh Kumar MR, Krishnan R, Sankar S, Unnikrishnan AS, Pai DS (2009) Increasing trend of "break-monsoon" conditions over India-role of ocean–atmosphere processes in the Indian Ocean. IEEE Trans Geosci Remote Sens Lett 6:332–336

Rodwell MJ, Hoskins BJ (1996) Monsoons and the dynamics of deserts. Q J R Meteorol Soc 122:1385–1404

Romatschke U, Houze RAJ (2011) Characteristics of precipitating convective systems in the South Asian monsoon. J Hydromet 12:3–26

Saeed S, Müller WA, Hagemann S, Jacob D (2011a) Circumglobal wave train and the summer monsoon over northwestern India and Pakistan: the explicit role of the surface heat low. Clim Dyn 37:1045–1060. https://doi.org/10.1007/s00382-010-0888-x

Saeed S, Müller WA, Hagemann S, Jacob D, Mujumdar M, Krishnan R (2011b) Precipitation variability over the South Asian monsoon heat low and associated teleconnections. Geophys Res Lett 38:L08702

Sardeshmukh PD, Hoskins BJ (1988) The generation of global rotational flow by steady idealized tropical convergence. J Atmos Sci 45:1228–1251

Sato T, Kimura F (2005) Impact of diabatic heating over the Tibetan Plateau on subsidence over northeast Asian arid region. Geophys Res Lett 32:L05809

Schumacher C, Houze RA, Kraucunas I (2004) The tropical dynamical response to latent heating estimates derived from the TRMM precipitation radar. J Atmos Sci 61:1341–1358

Sharmila S, Joseph S, Sahai AK, Abhilash S, Chattopadhyay R (2015) Future projection of Indian summer monsoon variability under climate change scenario: an assessment from CMIP5 climate models. Global Planet Change 124:62–78

Simmons A, Uppala S, Dee D, Kobayashi S (2007) ERA–Interim: new ECMWF reanalysis products from 1989 onwards. ECMWF Newsl 110:26–35

Stan C, Straus DM, Frederiksen JS, Lin H, Maloney ED, Schumacher C (2017) Review of tropical-extratropical teleconnections on intraseasonal time scales. Rev Geophys 55:902–937

Sundaram S, Krishnan R, Dey A, Swapna P (2010) Dynamics of intensification of the boreal summer monsoon flow during IOD events. Meteorol Atmos Phys 107:17–31

Umakanth U, Kesarkar AP, Rao TN, Rao S (2014) An objective criterion for the identification of breaks in Indian summer monsoon precipitation. Atmos Sci Lett 16:193–198

Vellore RK, Krishnan R, Pendharkar J, Choudhary AD, Sabin TP (2014) On the anomalous precipitation enhancement over the Himalayan foothills during monsoon breaks. Clim Dyn 43:2009–2031

Wang HJ (2002) The instability of the East Asian summer monsoon–ENSO relations. Adv Atmos Sci 19:1–11

Wang B, Wu R, Lau KM (2001) Interannual variability of the Asian summer monsoon: contrasts between the Indian and the western North Pacific-East Asian monsoons. J Clim 14:4073–4090

Wu R (2002) A mid-latitude Asian circulation anomaly pattern in boreal summer and its connection with the Indian and East Asian summer monsoon. Int J Climatol 22:1879–1895

Wu R, Wang B (2002) A contrast of the East Asian summer monsoon-ENSO relationship between 1962–77 and 1978–93. J Clim 15:3266–3279

Xie SP, Xu H, Saji NH, Wang Y, Liu WT (2006) Role of narrow mountains in large-scale organization of Asian monsoon convection. J Clim 19:3420–3429

Yanai M, Tomita T (1998) Seasonal and interannual variability of atmospheric heat sources and moisture sinks as determined from NCEP-NCAR reanalysis. J Clim 11:463–482

Yanai M, Esbensen S, Chu JH (1973) Determination of bulk properties of tropical cloud clusters from large-scale heat and moisture budgets. J Atmos Sci 30:611–627

Yasunari T (1986) Low-frequency interactions between the summer monsoon and the Northern Hemisphere westerlies. J Meteorol Soc Jpn 64:693–708

Yatagai A, Arakawa O, Kamiguchi K, Kawamoto H, Nodzu MI, Hamada A (2009) A 44-year daily gridded precipitation dataset for Asia based on a dense network of rain gauges. SOLA 5:137–140

Yatagai A, Kamiguchi K, Arakawa O, Hamada A, Yasutomi N, Kitoh A (2012) APHRODITE: constructing a long-term daily gridded precipitation dataset for Asia based on a dense network of rain gauges. Bull Am Meteorol Soc 93:1401–1415

Yu R, Wang B, Zhou T (2004) Tropospheric cooling and summer monsoon weakening trend over East Asia. Geophys Res Lett 31:L22212